Clim Dyn
DOI 10.1007/s00382-013-1670-7

A high-resolution ocean-atmosphere coupled downscaling of the present climate over California

Haiqin Li · Masao Kanamitsu · Song-You Hong · Kei Yoshimura · Daniel R. Cayan · Vasubandhu Misra

Received: 11 September 2012 / Accepted: 10 January 2013

Abstract A fully coupled regional ocean-atmosphere model system that consists of the regional spectral model and the regional ocean modeling system for atmosphere and ocean components, respectively, is applied to downscale the present climate (1985–1994) over California from a global simulation of the Community Climate System Model 3.0 (CCSM3). The horizontal resolution of the regional coupled modeling system is 10 km, while that of the CCSM3 is at a spectral truncation of T85 (approximately 1.4°). The effects of the coupling along the California coast in the boreal summer and winter are highlighted. Evaluation of the sea surface temperature (SST) and 2-m air temperature climatology shows that alleviation of the warm bias along the California coast in the global model output is clear in the regional coupled model run. The 10-m wind is also improved by reducing the northwesterly winds along the coast. The higher resolution coupling effect on the temperature and specific humidity is the largest near the surface, while the significant impact on the wind magnitude appears at a height of approximately 850-hPa heights. The frequency of the Catalina Eddy and its duration are increased by more than 60 % in the coupled downscaling, which is attributed to enhanced offshore sea-breeze. Our study indicates that coupling is vital to regional climate downscaling of mesoscale phenomena over coastal areas.

Keywords Regional climate · Coupled model · Ocean-atmosphere interaction · CCSM3 · RSM · ROMS

1 Introduction

The coupled system of the atmospheric-ocean general circulation models (AOGCMs) provides a good way to understand the response of the climate system to the increasing greenhouse gas concentrations and to project the future climate (Washington and Meehl 1989; Murphy 1995; Stouffer and Manabe 1999; Held and Soden 2006; Vecchi and Soden 2007; Ho et al. 2011). However, these global climate model systems suffer from relatively low resolutions with the horizontal resolution of most AOGCMs being approximately 200 km. A higher resolution simulation with a resolution of approximately 100 km, for example, improves the monsoonal characteristics over East Asia (Min and Jhun 2010), but the resolution is still too coarse to resolve mesoscale features along the coast.

For the reasons noted above, the regional climate models (RCMs) have been used to provide high-resolution simulations (e.g., Giorgi et al. 1994; Leung et al. 2004; Wang et al. 2004; Kanamaru and Kanamitsu 2008; Hong et al. 2010; Kanamitsu et al. 2010; Zhao et al. 2011). However, all of these studies suffer from low-resolution SST data relative to the resolution of RCMs. In other words, the availability of high-resolution ocean states is limited and

H. Li · M. Kanamitsu · D. R. Cayan
Scripps Institution of Oceanography,
University of California, San Diego, CA, USA

H. Li · V. Misra
Center for Ocean-Atmospheric Prediction Studies,
Florida State University, Tallahassee, FL, USA

S.-Y. Hong (✉)
Department of Atmospheric Sciences, College of Science,
Yonsei University, Seoul 120-749, Korea
e-mail: songyouhong@gmail.com

K. Yoshimura
Atmosphere and Ocean Research Institute,
University of Tokyo, Tokyo, Japan

Published online: 26 January 2013

even scarcer for climate projection and forecast. Therefore, the effects of regional-scale coastal ocean variability on the atmosphere are one of the uncertain components of regional climate projection. Many of the large cities of the world are located near the coast and therefore a better understanding of the air-sea interaction on coastal climate will have important societal implications.

The coupled ocean-atmosphere dynamic downscaling is a powerful and potentially effective approach to this unresolved problem. For example, Xie et al. (2007) coupled a regional atmospheric model with a basin scale oceanic GCM, and reproduced the salient features of the eastern Pacific climate at both the basin scale and the mesoscales. Likewise, the arctic warming as projected by the Rossby Centre Atmosphere Ocean climate model (RCAO), is obtained from downscaling the IPCC Fourth Assessment Report (AR4) Arctic future scenarios (Koenigk et al. 2011). Similarly, a regionally coupled ocean-atmosphere model is used to examine the sensitivity of a convective parameterization over the western North Pacific (Zou and Zhou 2011). The response and impact of the equatorial ocean dynamics and tropical instability waves in the tropical Atlantic under global warming conditions are investigated in the Scripps Coupled Ocean-Atmosphere Regional (SCOAR) model (Seo and Xie 2011). The ocean components in these studies are initialized using observed ocean climatology. In addition, the resolution of the atmospheric and oceanic components of the regional model in most of these studies is approximately 0.5°. However, we believe that a resolution of 0.5° is still insufficient to resolve the complex topography and coastal land-sea contrast.

A fully coupled regional ocean-atmosphere model, which includes the Regional Spectral Model (RSM; Juang and Kanamitsu 1994; Juang et al. 1997; Kanamitsu et al. 2010) as the atmospheric component and Regional Ocean Modeling System (ROMS; Haidvogel et al. 2000; Shchepetkin and McWilliams 2005) as the oceanic component, was developed to execute the Coupled California Reanalysis downscaling at 10 km (CCaRD10; Li et al. 2012). This regional coupled model is designed for the practical application of the coupled downscaling of the reanalysis, as well as the high-resolution regional climate projection and seasonal forecast. Li et al. (2012) demonstrated that this regional coupled model tends to generate a near-realistic ocean state, and shows some superiority in simulating higher moments of the SST compared to the 1° reanalysis SST. In this study, this coupled system is used to downscale the CCSM3 oceanic and atmospheric output to further reveal the impact of the coupling along the California Coast.

The global oceanic and atmospheric forcing, regional coupled model and methodology are described in Sect. 2. In Sect. 3, the results of the coupled downscaling are presented followed by conclusions in Sect. 4.

2 Experimental setup

The atmospheric and oceanic large-scale boundary conditions are provided by the global coupled model of the National Center for Atmospheric Research (NCAR) Community Climate System Model 3.0 (CCSM3), which includes the NCAR Community Atmospheric Model (CAM) and the Parallel Ocean Program (POP) oceanic model. The present climate (1985–1994) is from the climate of the twentieth century CCSM3 experiment. All of the data are available from the NCAR Earth System Grid (http://www.earthsystemgrid.org/dataset/ucar.cgd.ccsm.b30.030e.html). The CAM outputs are in T85 horizontal resolution of 26 hybrid vertical levels. The POP 3-D ocean state are in 384 × 320 irregular horizontal global grids and 40 vertical levels, while the POP SST provided by Earth System Grid is in T85, which is the same as in CAM.

The regional coupled model for CCaRD10 is used in this study. A brief outline of this regional coupled model is provided here. Readers are directed to Li et al. (2012) for a more detailed description of the model. The RSM is a primitive equation atmosphere model. ROMS is a free-surface, terrain-following, primitive equations ocean model. The RSM and ROMS share the same domain and resolution. In addition, they are coupled in parallel mode. The two independent executable jobs of the RSM and the ROMS run at the same time. The air-sea coupling interval is 24 h. The atmospheric forcing from the RSM is directly utilized by the ROMS and the ROMS provides the SST to the RSM without a SST-flux coupler. This high-resolution coupled system is applied for the downscaling of the CCSM3 ocean and atmosphere outputs.

The 6 hourly CAM 26 hybrid pressure level atmospheric fields are interpolated to 28 sigma levels following the study by Yoshimura and Kanamitsu (2009), but without vertical incremental interpolation. The monthly irregular grid POP ocean fields are interpolated to 320 × 192 regular grid in order to use the existing pre-processing programs.

Two sets of experiments are designed with the regional coupled ocean-atmosphere model. The control run is the 10-years uncoupled RSM run forced by 6-hourly CAM atmospheric forcing and daily POP SST, which was post-processed to T85 (∼1.4°) from Earth System Grid. The control experiment is referred to as the UNCPL experiment in this paper. In the coupled experiment, the RSM is forced by 6-hourly CAM atmospheric forcing and the ROMS is forced by the monthly POP 3-D oceanic boundary conditions. The coupled experiment is referred to as the CPL

experiment in this paper. The POP monthly mean SST and the net heat flux sensitivity term computed from the UNCPL experiment are used in the ROMS built-in correction scheme (Marchesiello et al. 2003) in order to avoid the large scale SST drift in the CPL run. The model configuration including the regional model domain, and the spatial resolution (10 km) are the same as in the study by Li et al. (2012). The model domain is shown in Fig. 1. The SST climatology will be displayed in domain A. The SST variation and other coastal coupling effects will be analyzed within the smaller domain B. The vertical coupling impact on the atmosphere is studied in the smallest domain C. The data from the first 2 years is discarded in order to account for the spin-up as in the CCaRD10. The remaining 8 years (1987–1994) of the regional simulation are used in the analysis.

The Cooperative Observer Program (COOP, http://www.nws.noaa.gov/os/coop/) station data, the buoy observation from the National Data Buoy Center (http://www.ndbc.noaa.gov/), the 4-km pathfinder V5 AVHRR high resolution blended SST (ftp://podaac-ftp.jpl.nasa.gov/allData/avhrr/L3/pathfinder_v5/monthly/), California reanalysis downscaling at 10 km (CaRD10, Kanamitsu and Kanamaru 2007) are used to verify the performance of the coupled downscaling.

3 Results

3.1 Sea surface temperature (SST)

3.1.1 Seasonal climatology

Figure 2 compares the summer and winter climatology (1987–1994) from a 4-km AVHRR observed SST, the CCSM3 SST used for the UNCPL experiment, and the simulated SST from the CPL run. In the summer, an upwelling cold tongue is seen in the 4-km AVHRR observed SST (Fig. 2a) and the CPL SST (Fig. 2c). This upwelling phenomenon along the coast of California in summer is not captured well by the CCSM3 global coupled model, which may be due to the coarse resolution. This bias results in the unrealistic zonal SST gradient to the west of Baja California, with a significant warm bias (Fig. 2b). This warm bias is alleviated significantly by the coupled downscaling (Fig. 2c). The summer SST is quantitatively evaluated against the buoy observation over the buoy station of Half Moon Bay (37.36°N, 122.88°W) within the upwelling region. The CCSM3 SST has a warm bias of 10.30 °C, while the CPL SST has a cold bias of only −1.13 °C. In winter, the SST of the coupled run (Fig. 2f) tends to be a little colder over the Bight of Southern

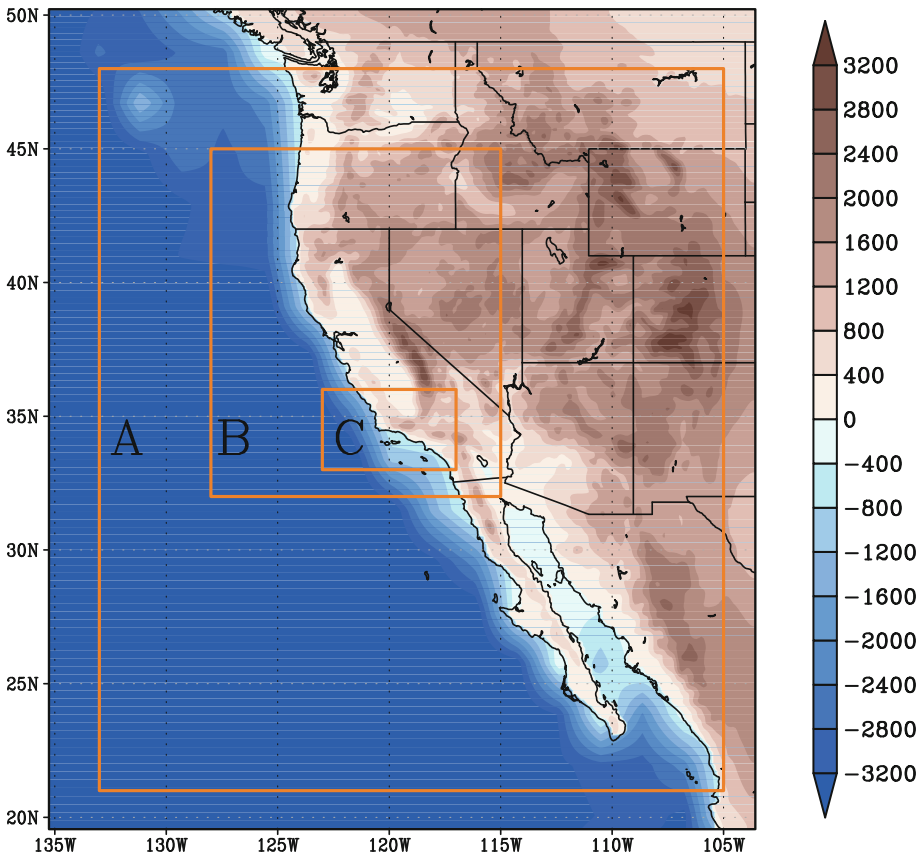

Fig. 1 The model domain, land topography and ocean bathymetry (m). Domain A is used to examine the large-scale pattern of the SST. The impact of the coupling on California is examined in the middle domain B. The smallest domain C is used to study the coupling impact on the *vertical* atmosphere

California than AVHRR (Fig. 2d) and CCSM3 SST (Fig. 2e). It is quantitatively evaluated against buoy observation over the buoy station of Santa Monica Basin (33.75°N, 119.08°W) in the Bight of Southern California. The CPL SST has a cold bias of −1.46 °C, while the CCSM3 SST has a warm bias of 0.72 °C. A similar cold bias is also noted in the winter season in the CCaRD10.

3.1.2 Monthly variations

In order to examine the variability of the SST on a monthly scale, the monthly SST variance from the AVHRR, CCSM3 and CPL simulation in the summer and winter seasons are computed (Fig. 3).

In the summer, the observed AVHRR SST variance is greater than 0.7 °C along the coast, and the intensity of variance decreases offshore (Fig. 3a). There is a wide offshore band of a low SST variance from CCSM3 in the order of 0.3 °C (Fig. 3b), while the pattern and intensity of the SST variance from CPL run (Fig. 3c) is comparable to that of the AVHRR observation. In the winter, the observed AVHRR SST varies by approximately 0.6 °C along the coast (Fig. 3d). The CCSM3 SST variance is only approximately 0.4 °C (Fig. 3e) and the SST variance form the CPL simulation (Fig. 3f) is much larger than that from the observation and CCSM3 SST. Since the upwelling season is from May to September over California and the upwelling phenomenon is well resolved by CPL, the monthly SST variability is more dramatically improved by the CPL simulation than the CCSM3 in summer.

3.2 Surface atmospheric fields

3.2.1 Seasonal cycle of 2-m air temperature (T2m)

The COOP station of San Francisco (37.775°N, 122.418°W) over Central California and the nearby buoy station of Half Moon Bay (37.36°N, 122.88°W), as well as the COOP station of Los Angeles (32.715°N, 117.156°W) over Southern California and the nearby buoy stations of Santa Monica Basin (33.75°N, 119.08°W) are selected in order to examine the seasonal variation in the 2-m air temperature. It is evident that the seasonal cycle displayed by the monthly T2m series from the CPL run matches the

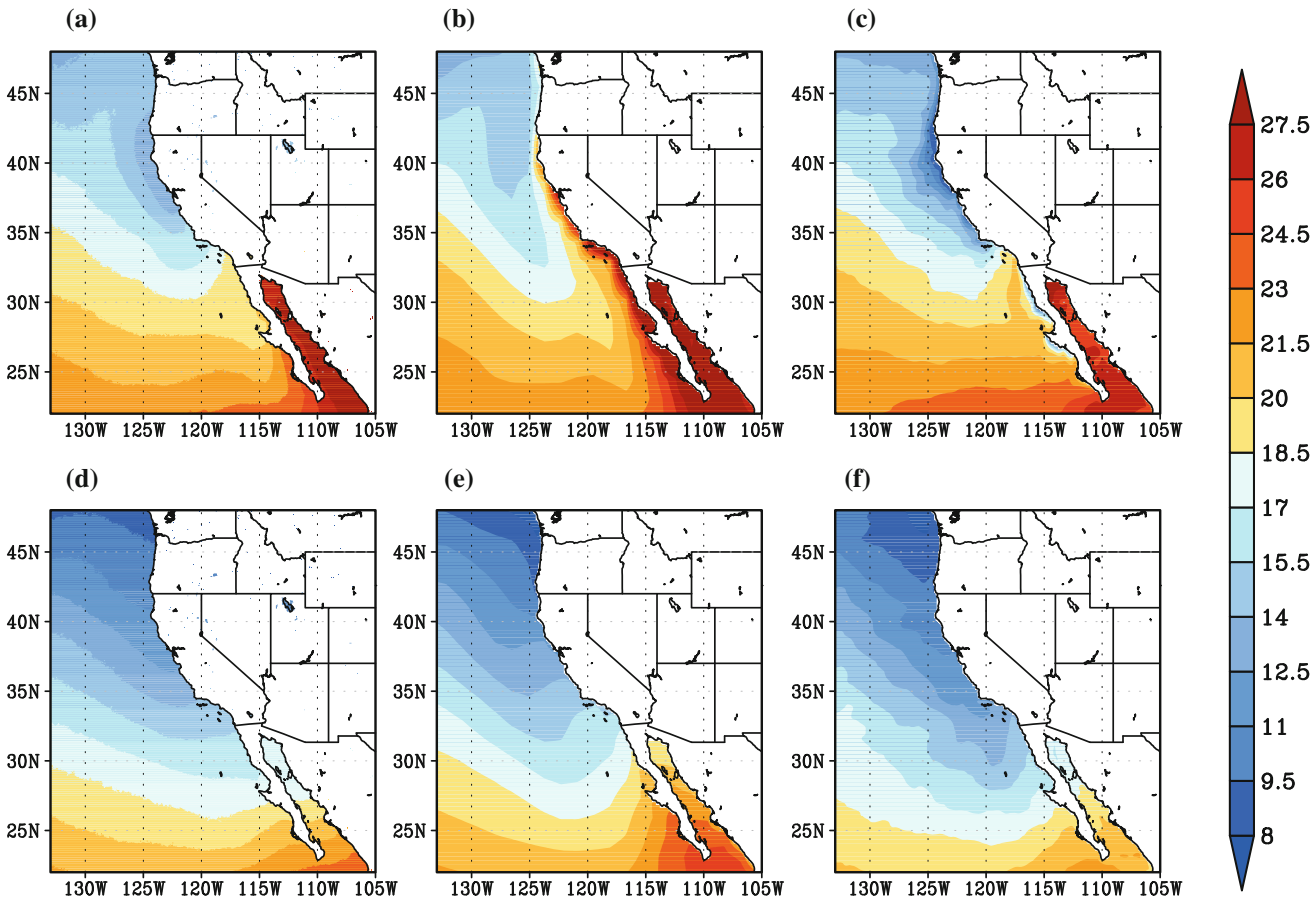

Fig. 2 Summer SST climatology (°C) from **a** AVHRR, **b** CCSM3, and **c** CPL; and the winter SST climatology from **d** AVHRR, **e** CCSM3, and **f** CPL

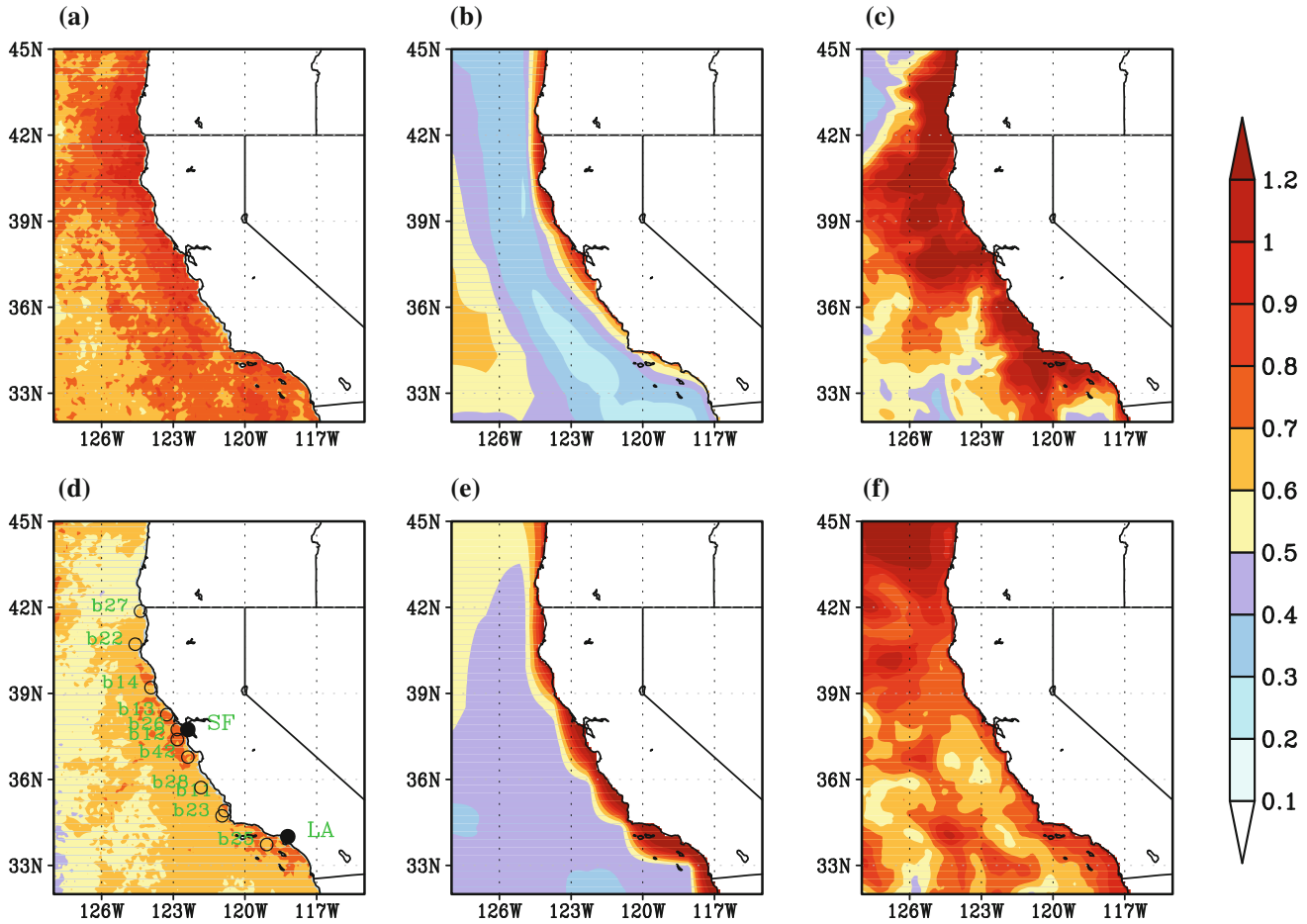

Fig. 3 Monthly SST variance (°C) in summer from **a** AVHRR, **b** CCSM3, and **c** CPL; and monthly SST variance (°C) in winter from **d** AVHRR, **e** CCSM3, and **f** CPL. The buoy stations (*white circle*) and COOP stations (*solid circle*) are shown in (**d**)

buoy observation very well over Half Moon Bay, whereas the seasonal variation in the T2m in the UNCPL experiment is much stronger than the buoy observation (Fig. 4a). These characteristics were confirmed from the comparison of a monthly time series of T2m for whole years (Figures not shown). In the winter months, the deviation in the UNCPL T2m from the buoy observation is small. The deviation then becomes larger and larger during the upwelling season (May to September). The seasonal cycle of the T2m in the UNCPL also deviates from the COOP observation over San Francisco from May to September, while the seasonal cycle of T2m from CPL run is much closer to the observation (Fig. 4b). A similar situation is also seen over the COOP station of Los Angeles (Fig. 4d) and the nearby station of Santa Monica Basin (Fig. 4c). It is indicated that the CCSM3 SST with coastal warm bias appears to cause the unrealistic coastal T2m intra-annual variation in the UNCPL experiment, which is largely corrected by the high-resolution coupling.

3.2.2 10 m surface winds

In summer, the equatorward alongshore wind (Fig. 5a, b), prevails along the coast of California. The wind speed from CaRD10 is about 6 m/s along the coast of California, while it is significantly overestimated by the UNCPL run in about 9 m/s, following the CCSM3 boundary forcing. The summer wind vector difference between the CPL and UNCPL experiments is northwestward, and the wind speed bias in the UNCPL run is reduced by as much as 1.5 m/s along the coast by the coupled downscaling (Fig. 5c). In the winter, the observed westerly wind blows from the Pacific Ocean and separates into northward and southward branches at the coast of Central California (not shown). The winter wind difference is not as large as in the summer, but the apparent onshore wind vector difference is seen over the South California Bight (Fig. 5d), which should be caused by the SST difference between CPL (Fig. 2f) and CCSM3 (Fig. 2e).

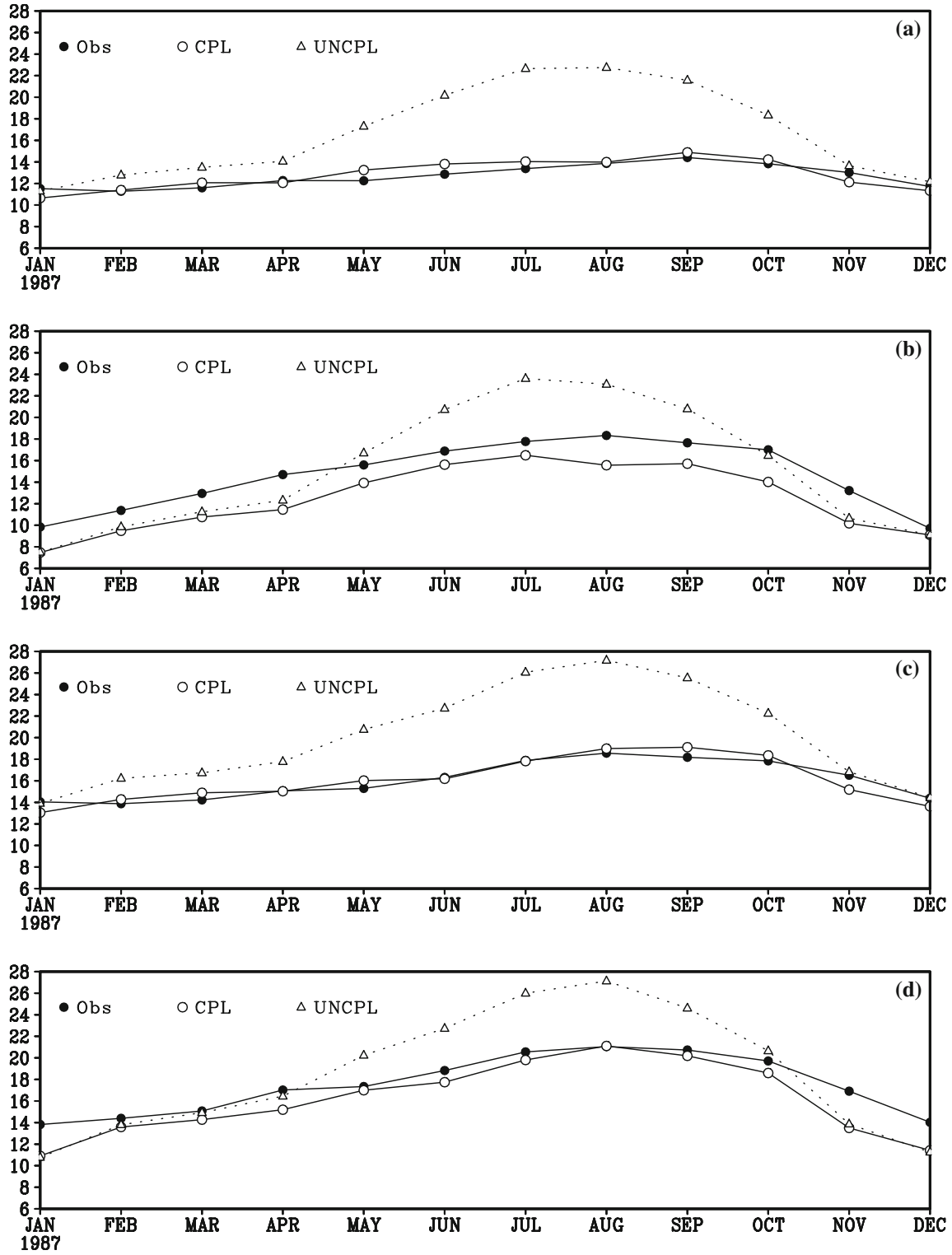

Fig. 4 Monthly T2m climatology (°C) from observation, CPL and UNCPL over **a** buoy station of Half Moon Bay (37.36°N, 122.88°W), **b** COOP station of San Francisco (37.775°N, 122.418°W), **c** buoy station of Santa Monica Basin (33.75°N, 119.08°W), and **d** COOP station of Los Angeles (32.715°N, 117.156°W)

In order to quantitatively evaluate the wind speed, the bias and root mean square error (RMSE) of the UNCPL and CPL monthly wind speed in comparison with buoy observations are computed in the summer months (Table 1). It is seen that the wind speed bias and RMSE from CPL is almost reduced over each station. In June, the

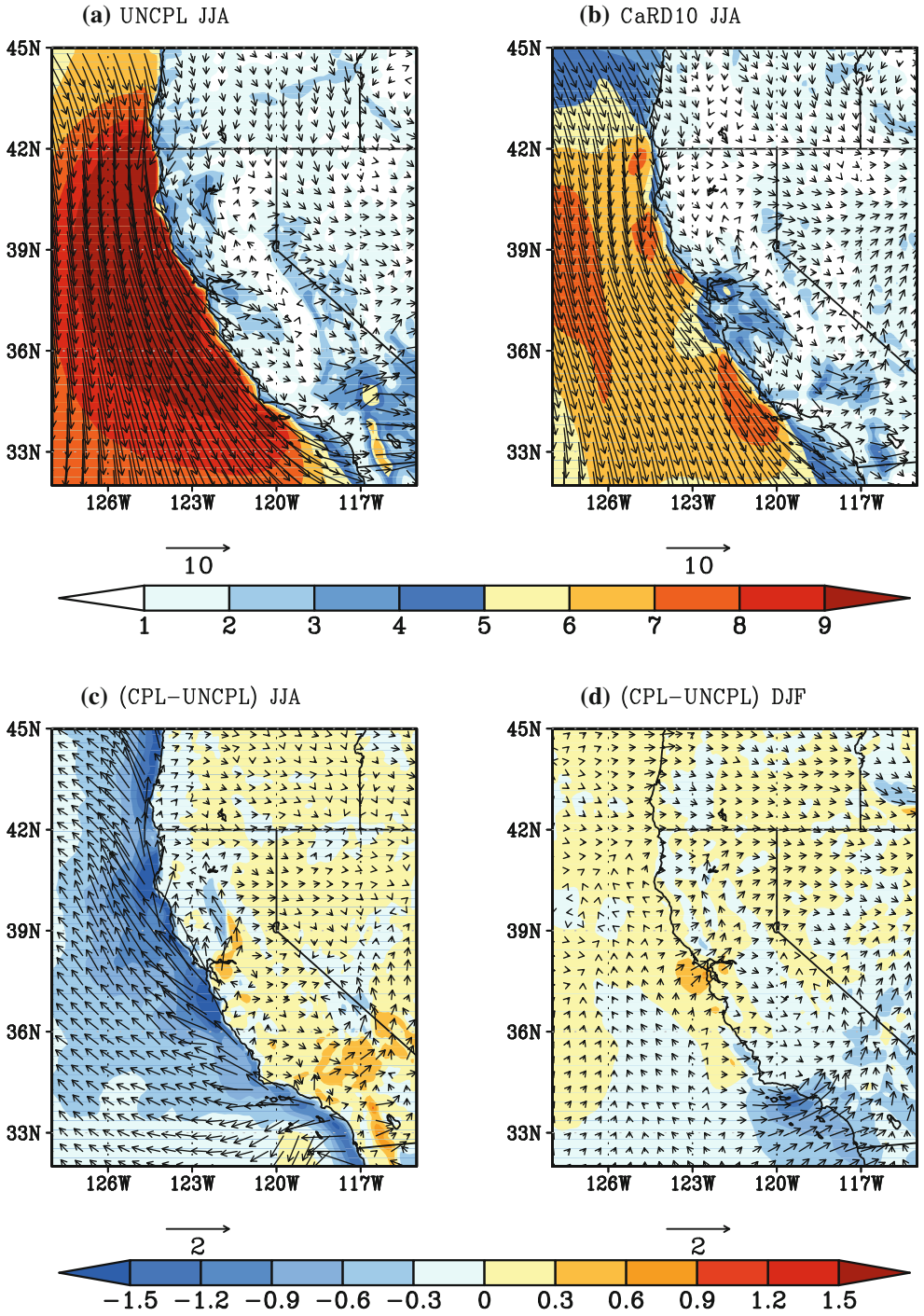

Fig. 5 Climatology of 10-m wind vector and wind speed (m/s) from CPL in **a** summer and **b** winter; and the difference between the CPL and UNCPL in **c** summer, and **d** winter

average wind speed bias from the UNCPL is 3.29 m/s, and this bias is only 2.02 m/s in the CPL experiment. The average RMSE from the UNCPL run in June is 4.04 m/s, which is reduced to 3.16 m/s in the CPL run. In July, the average wind speed bias and RMSE from the UNCPL are 4.87 and 5.04 m/s. In contrast, the average bias and RMSE from the CPL are only 3.53 and 3.77 m/s, which is a 27.5 and 25 % reduction respectively. In August, the average bias and RMSE from the UNCPL are 4.99 and 5.45 m/s, and they are reduced to 3.77 m/s (a 24.5 % reduction) and 4.29 m/s (a 21 % reduction) in the CPL experiment. The wind speed difference in winter months between CPL and UNCPL is not as apparent as in summer months. The difference in the surface air temperature for the CPL and

UNCPL leads to a wind difference. The surface wind may also increase (decrease) over warm (cold) water in association with a decrease (increase) in the stability of the boundary layer (Chelton and Xie 2010).

3.3 Atmospheric structure

Since the unrealistic warm near surface temperature bias from CCSM3 is significantly reduced by the CPL run, the smallest domain C is selected to study the impact on the vertical structure of the atmosphere. The vertical profiles of the summer climatology temperature (°C), specific humidity (g/kg), and wind speed (m/s) from the UNCPL and CPL experiments relative to the CaRD10 over the ocean and land portion of domain C are shown in Fig. 6.

3.3.1 Temperature

Over the ocean portion of domain C, the 1,000-hPa temperature climatological difference from the UNCPL in comparison with the CaRD10 is 2.23 °C and it is approximately −1.20 °C in the CPL run (Fig. 6a). The temperature difference between the CPL and UNCPL is as high as 3.43 °C at 1,000 hPa. It should also be noted that the domain averaged temperature difference between the CPL and UNCPL is reduced upward.

Over the land portion of domain C, the 1,000-hPa temperature climatological difference of the UNCPL in comparison with the CaRD10 is 2.01 °C and the domain averaged climatological temperature difference between the CPL and CaRD10 is 0.98 °C (Fig. 6d). It is also interesting to note that the temperature difference between the CPL and UNCPL over land is 1.03 °C, which is much smaller than that over the ocean. The domain averaged difference between the CPL and UNCPL is also diminished upward from 1,000 hPa.

3.3.2 Specific humidity

Over the ocean portion of domain C, the 1,000-hPa specific humidity difference between the UNCPL and the CaRD10 is 1.36 g/kg, and the difference between the CPL and the CaRD10 is −1.49 g/kg (Fig. 6b). The specific humidity difference between the CPL and UNCPL is as large as −2.85 g/kg at 1,000 hPa and it decreases upward.

Over the land portion of domain C, the 1,000-hPa specific humidity difference from the UNCPL is 0.04 g/kg, and the difference between the CPL and the CaRD10 is −2.11 g/kg (Fig. 6e). The humidity difference between the CPL and the UNCPL is as large as −2.15 g/kg at the 1,000-hPa height, with diminishing differences as it move upward.

3.3.3 Wind speed

Over the ocean portion of domain C, the difference in the wind magnitude at 1,000 hPa between UNCPL and CaRD10 is 1.78 m/s. In addition, the wind speed difference at 1,000 hPa between CPL and CaRD10 is 1.53 m/s (Fig. 6c). The difference in the domain averaged wind speed between the CPL and the UNCPL is only −0.25 m/s. However, the difference in wind speed between the CPL and the UNCPL becomes 0.41 m/s at the 925 hPa level. The difference in wind speed between the CPL and UNCPL experiments is further increased to 0.58 m/s at the 850-hPa level, with a decreasing difference further upward. Over the land portion of domain C, the difference in wind speed between the CPL and the UNCPL is also smaller at

Table 1 Bias (RMSE) of the monthly wind speed in comparison with buoy observation (m/s)

Buoy station	June		July		August	
	UNCPL	CPL	UNCPL	CPL	UNCPL	CPL
b11	2.34 (3.08)	1.21 (2.25)	2.58 (3.06)	1.57 (2.05)	2.50 (3.17)	1.76 (2.40)
b12	5.00 (5.53)	3.68 (4.63)	7.03 (7.24)	5.54 (5.75)	7.42 (7.52)	6.10 (6.17)
b13	2.47 (2.86)	1.48 (2.02)	5.61 (5.53)	4.59 (4.61)	6.43 (6.79)	5.57 (5.96)
b14	3.61 (3.89)	2.17 (2.67)	6.82 (6.95)	4.92 (5.11)	7.40 (7.69)	5.48 (5.74)
b22	6.21 (6.88)	4.52 (5.26)	7.91 (7.89)	5.68 (5.65)	8.56 (8.65)	5.95 (6.14)
b23	0.80 (2.54)	−0.31 (2.56)	1.65 (1.96)	0.74 (1.25)	0.88 (2.34)	0.22 (2.06)
b25	4.49 (4.53)	2.96 (3.03)	2.59 (2.49)	1.41 (1.43)	2.64 (2.59)	1.60 (1.58)
b26	3.40 (4.02)	2.28 (3.13)	5.70 (5.71)	4.39 (4.47)	5.65 (5.77)	4.46 (4.59)
b27	3.63 (3.89)	3.04 (3.38)	4.81 (5.13)	4.06 (4.27)	5.29 (5.78)	4.54 (5.13)
b28	2.19 (3.78)	0.93 (3.24)	4.34 (4.72)	3.50 (3.97)	4.17 (4.96)	3.76 (4.58)
b42	2.08 (3.43)	0.31 (2.64)	4.52 (4.73)	3.47 (2.86)	3.96 (4.64)	2.08 (2.84)
Average	3.29 (4.04)	2.02 (3.16)	4.87 (5.04)	3.53 (3.77)	4.99 (5.45)	3.77 (4.29)

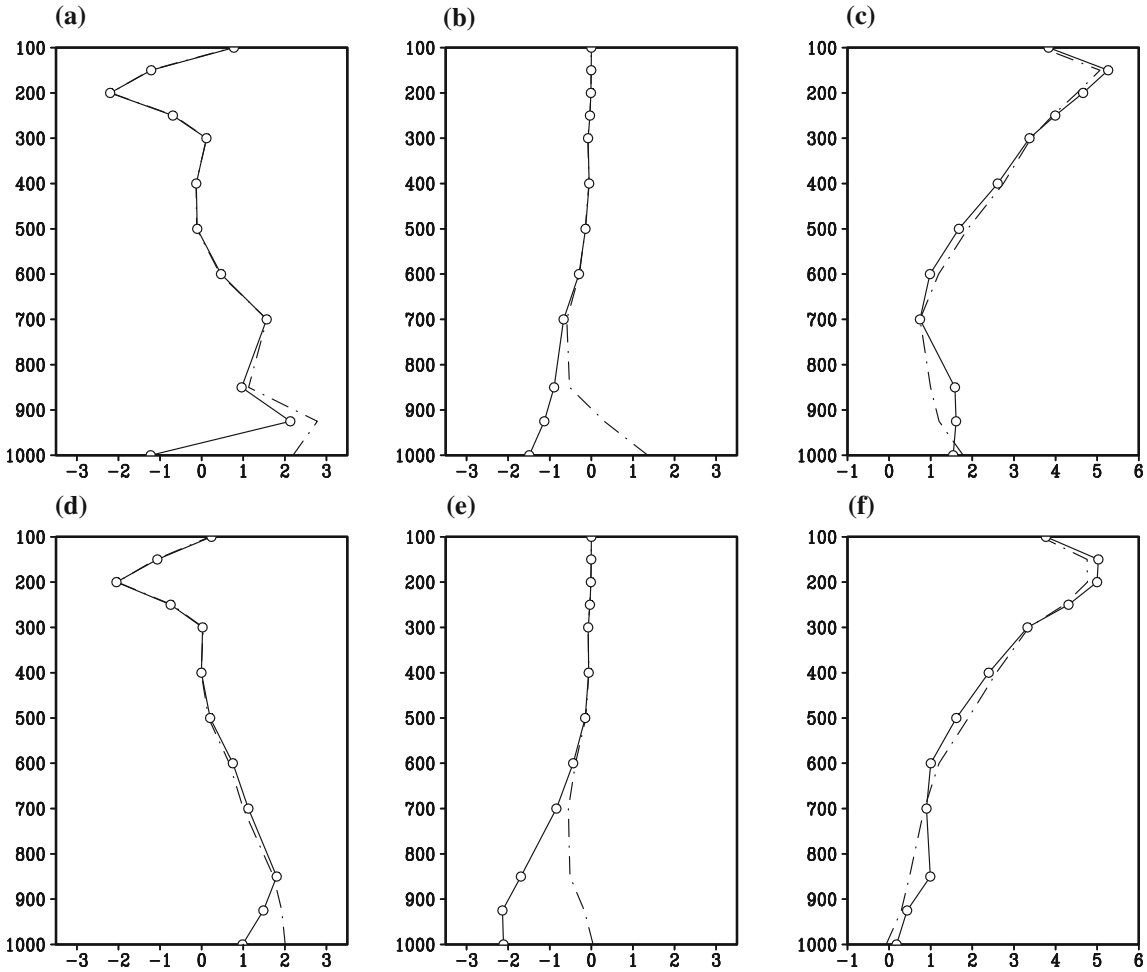

Fig. 6 *Vertical* profiles from UNCPL (*dashed line*) and CPL (*solid line with open circle*) in comparison with the CaRD10 of **a** temperature (°C), **b** specific humidity (g/kg) and **c** wind magnitude (m/s) over the ocean portion of domain C, and **d** temperature (°C), **e** specific humidity (g/kg) and **f** wind magnitude (m/s) over the land portion of domain C

the 1,000-hPa level at −0.07 m/s, and the difference is largest at the 850-hPa level at 0.5 m/s (Fig. 6f).

It is seen that the differences for some variables penetrate up to about 700 hPa, which could be due to the interaction between the surface layer and PBL in the atmosphere, although the SST difference is the only forcing [refer to Hong and Pan (2000) for the impact of soil moisture on the vertical profiles of atmosphere]. Also, the penetration depth of the differences is deeper for moisture and winds than for temperature, which is consistent with the PBL mechanism in previous studies (e.g., Hong et al. 2006). Again, these differences in atmosphere are caused by the combined effect of coupling and resolution in the CPL run.

3.3.4 Planetary boundary layer height (PBLH)

Given the large SST bias along the coast of California in the CCSM3 (see Sect. 3.1), it would be further illuminating to examine the PBLH from the UNCPL and CPL experiments. The NCEP/NCAR reanalysis (Kalnay et al. 1996) downscaling of the CaRD10, which is forced by the observed SST, is available from 1948 to 2011. Therefore, it is used as the reference to examine the PBLH in this study. The relative differences in the summer climatology of the PBLH (expressed in percentage) in the UNCPL and in the CPL experiments from the corresponding climatology in CaRD10 are shown in Fig. 7. The PBLH from the UNCPL run is overestimated along the coastal area of California in comparison with the CaRD10 (Fig. 7a). The difference in the PBLH along the coastline is as large as 250 m, which is approximately a 100 % overestimation (Fig. 7a). In contrast, the climatological difference in the PBLH between the CPL run and the CaRD10 is relatively small along the coastal ocean and over the coastal land (Fig. 7b) in comparison with the UNCPL run (Fig. 7a). The SST difference relative to CaRD10 from UNCPL (Fig. 7c) and CPL (Fig. 7d) over the coastal area matches the pattern of PBLH

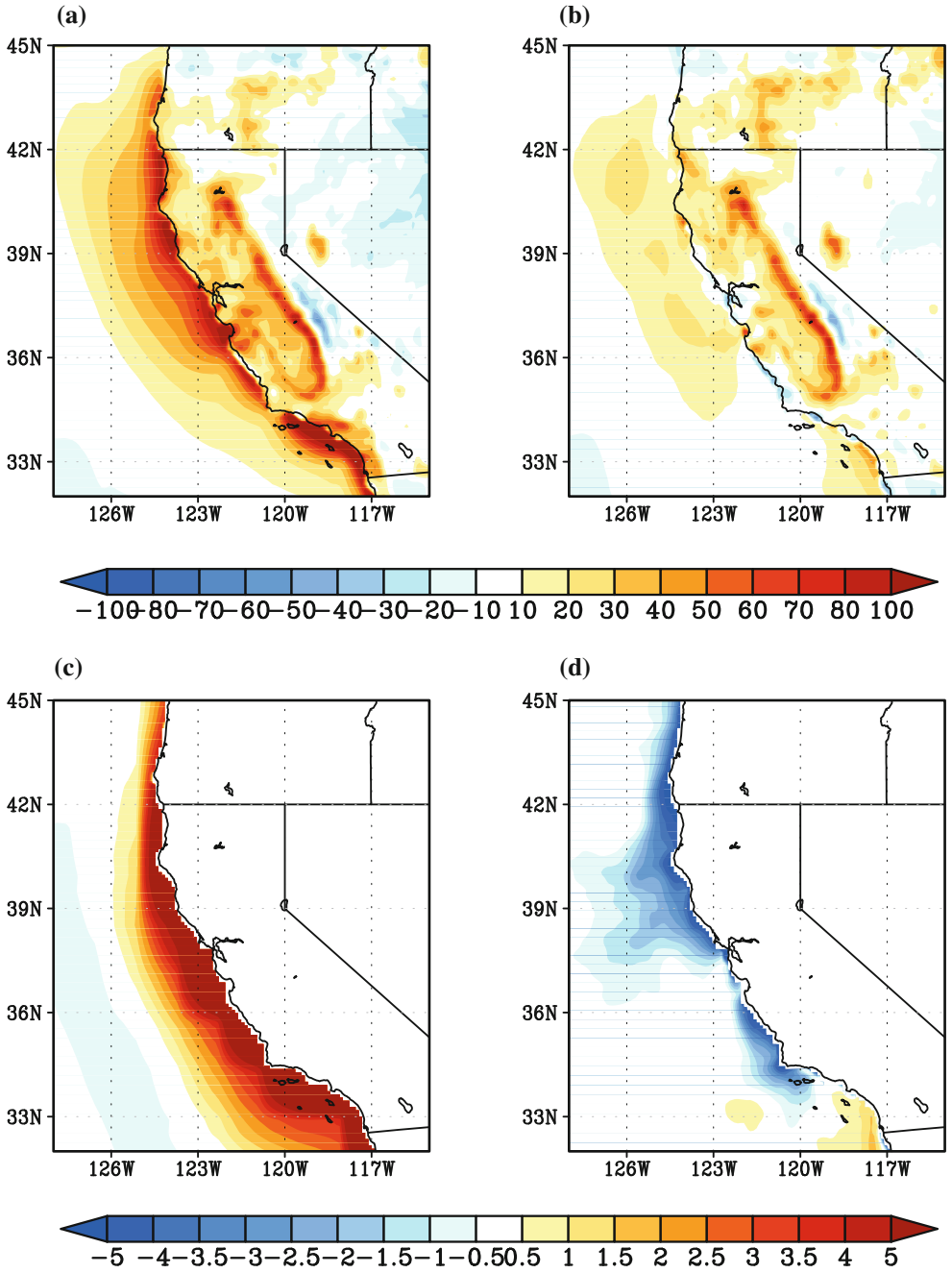

Fig. 7 The relative difference of PBLH (in percentage) in comparison with the CaRD10 from **a** UNCPL and **b** CPL, and the SST difference (°C) relative to CaRD10 from **c** UNCPL and **d** CPL in summer climatology (1987–1994)

difference. It is suggested that the large bias in the PBLH from the UNCPL experiment is forced by the relatively large warm bias in the SST from the CCSM3 experiment. A physical reasoning for the PBLH difference can be deduced from the fact that the PBLH of Hong and Pan (1996) used in this study is determined by the virtual temperature at the lowest model level of RSM, which is directly coupled with the SST. Also, the significant difference over land is presumably due to the non-linear effects (e.g., advection) in response to the influence of resulting SST.

3.4 Catalina Eddy

When the regular northwesterly flow changes direction and turns into a southerly flow along the coast of the Southern California Bight, a mesoscale circulation called Catalina Eddy (CE) is produced (Bosart 1983; Mass and Albright

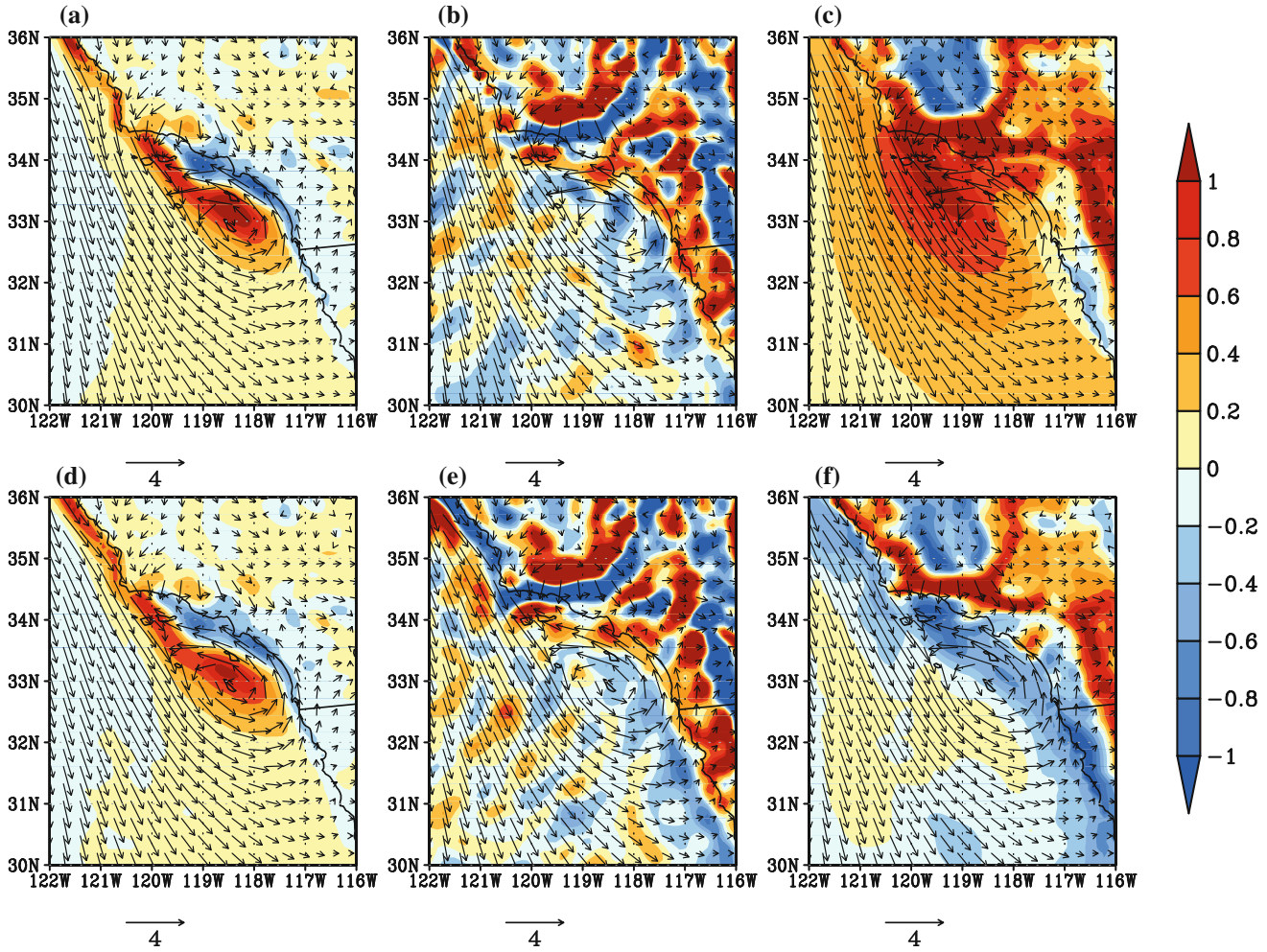

Fig. 8 Composite anomaly of **a** vorticity (10^{-4} s^{-1}), **b** divergence (10^{-4} s^{-1}) and **c** T2m (°C) from the UNCPL; and composite anomaly of **d** vorticity (10^{-4} s^{-1}), **e** divergence (10^{-4} s^{-1}) and **f** T2m (°C) from the CPL. The composite anomaly of the 10-m wind vector is overlapped

1989; Mass and Steenburg 2000). It has several important meteorological implications including a change in visibility, the occasional production of light rain, a variation in pollution, and the lowering of coastal temperature.

Kanamitsu et al. (2013) analyzed the climatological properties, dynamical and thermodynamical characteristics, and long-term variabilities of the Catalina Eddy over 61 years (1948–2008) with hourly CaRD10 data. Some new findings were gained from the large number of CE cases in the CaRD10. Kanamitsu et al. (2013) found that large-scale cyclonic/anticyclonic forcing is not necessary for eddy formation and there is no apparent north-south pressure gradient anomaly that drives the southerly flow during life cycle of CE, while all of the previous studies focused on the strong eddy and concluded that large-scale forcing was crucial. The onshore/offshore of the sea-breeze is essential for the CE formation and decay. Using the same CE detection method as in Kanamitsu et al. (2013), Li et al. (2012) found an additional 6.5 % CE hours in the coupled downscaling of the reanalysis than the uncoupled downscaling of the same global reanalysis.

In this study we use the 10-m wind fields from the canonical eddy to detect CE cases in the CPL and the UNCPL experiments following the methods of Kanamitsu et al. (2013) and Li et al. (2012). The spatial pattern correlation between the composite near surface wind directions and the hourly CPL and UNCPL 10-m wind directions are then calculated within 32°N–34°N, 121°W–117°W. The Pearson product-moment correlation coefficient is used here since we are only interested in the direction of the winds, not the amplitude. It is still assumed that a CE occurred if the correlation coefficient is larger than the threshold of 0.7, which represents significant cyclonic rotation over the Bight of Southern California.

Table 2 The number of detected Catalina Eddy hours and the duration (in hours) of the Catalina Eddy events in the UNCPL and CPL runs

Years	CE hours		CE events durations		
	UNCPL	CPL	Duration	UNCPL	CPL
1987	195	400	1	110	145
1988	218	339	2	82	143
1989	198	355	3	60	109
1990	171	323	4	55	88
1991	225	346	5	37	70
1992	245	324	6	41	51
1993	237	351	7	15	41
1994	205	396	Over 8	51	80
Total	1,694	2,834	Total	451	727

The primary characteristics of the detected CE anomaly composite from the UNCPL and CPL experiments are shown in Fig. 8. The anomalies are computed by subtracting the 8-year hourly mean of the variable in order to eliminate the climatological diurnal variability that appears in the anomaly field. The composite near-surface structure of the eddy is characterized by elongated positive vorticity emanating from Point Conception, with a narrow band of negative vorticity along the coast (Fig. 8a, d). A belt of convergence is observed along the coast of Southern California (Fig. 8b, e). The warm T2m anomaly from the UNCPL is strong to the west of the CE, and is weak to the east of the CE (Fig. 8c). However, the T2m anomaly from the CPL is a little warm to the west of CE, but is much colder to the east of the CE and along the coast (Fig. 8f). This coastal cold tongue is also noted in the numerical simulations of Ulrickson et al (1995), Kanamitsu et al. (2013), and Li et al. (2012). According to the vorticity budget study with the composite CE events (Kanamitsu et al. 2013), the source of the eddy is the vorticity generated by the convergence along the coast of the Santa Barbara Channel. It is then advected to the southeast of the Bight region, where it interacts with another vorticity generation source along the coast from the coastal convergence caused by the offshore sea breeze circulation. Approximately 6 h (06 UTC or 10:00 p.m. LST) before the mature stage of the CE, the sudden generation of positive vorticity (stretching term) occurs along the coast. This is caused by the convergence due to the sea-breeze changing from onshore to offshore. At the same time, negative vorticity is generated close to the coastline primarily due to the horizontal advection of the negative vorticity from land. Since the generating of positive vorticity leading to pressure falls and a cyclonic circulation simultaneously (Carson 1998), the northerly wind would turn to southerly wind. This combined positive and negative vorticity region resulted in the formation of southerly flow along the coast.

The detected Catalina Eddy hours from the CPL and UNCPL experiments during the 8 analyzed years (1987–1994) are listed in Table 2. A total of 1,694 CE hours are detected in the UNCPL run, while 2,834 CE hours are observed in the CPL run. There were 451 and 727 CE events identified in the UNCPL and the CPL runs, respectively. The CPL run tends to generate 67.3 % more CE hours and 61.2 % more CE events than the UNCPL experiment. In this study, the coastal SST in the CPL run is much colder than that in the UNCPL experiment during the upwelling season (May to September). In addition, the stronger land-sea surface temperature gradient in the CPL run (Fig. 8f) enhances the offshore flow over the coastal area of the Southern California Bight. The stronger offshore sea-breeze helps the development of CE in the CPL run. The 67.3 % additional CEs hours in the CPL than the UNCPL are attributed to this difference in the sea-breeze circulation. The increase in the CE events is observed for each-hour long duration (Table 2). The accumulated CE hours appear more in the May–September periods, and the increased CE hours in the CPL in comparison with the UNCPL are also greater in May–September, when the upwelling is at a seasonal peak in summer (Fig. 9a).

The life cycle of the CE is related to local time and sea-breeze circulation (Kanamitsu et al. 2013). The eddy abruptly develops in the early evenings and reaches its full-development stage by midnight. It maintains its intensity until the early morning and then it decays in the late afternoon. The accumulated CE hours in the diurnal time from the UNCPL and CPL runs (Fig. 9b) also show that the eddy reaches its maximum between 4 a.m. and 11 a.m. LST, and there are very few CE hours in the afternoon (2 p.m. to 8 p.m. LST). The increased CE hours in the CPL run are also observed during local night and morning time (Fig. 9b).

It is noted that there is no validation of the CE in terms of its duration and frequency, because there are not reliable long term observed datasets. Therefore, a direct evaluation of the simulated results in this study is not possible. The increased number and duration of the CE in the CPL run is argued to be more realistic given that the climatological SST as well as the atmospheric structure and its variations are closer to the observation than in the uncoupled experiment (UNCPL). It is further mentioned that the high resolution air-sea coupling plays an important role in the development of coastal mesoscale circulation over the Southern California Bight.

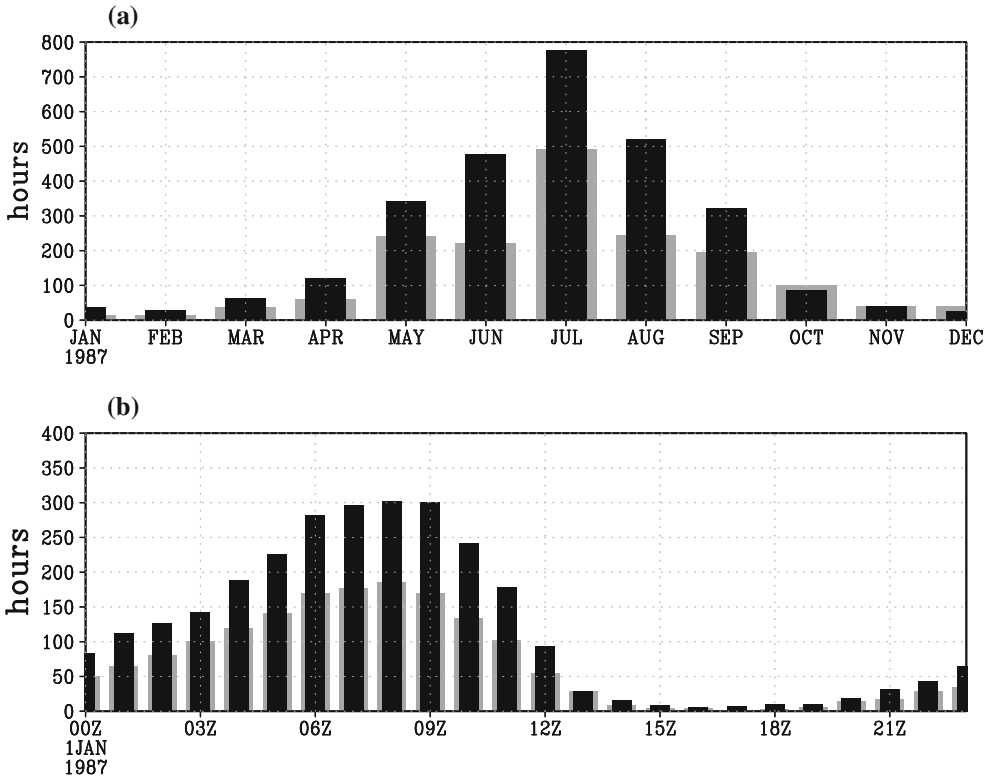

Fig. 9 Accumulated Catalina Eddy hours in **a** annual cycle months, and **b** diurnal cycle hours (local Pacific Standard Time). The UNCPL is in *grey*, and CPL is in *black*

4 Conclusions

As an extension to the Coupled California Reanalysis Downscaling at 10 km (CCaRD10, Li et al. 2012), a 10-year ocean-atmosphere coupled downscaling of the present climate from CCSM3 experiments was executed over the same domain. All of the model configurations of this study are the same as in the CCaRD10, except for the oceanic and atmospheric initial/boundary conditions. The first 2 years of the coupled downscaling in this study are discarded due to ocean spin-up as in the CCaRD10, and the remaining 8 years are used for the analysis. The analysis focuses on the coastal areas of California.

It is shown that the CCSM3 simulation exhibits a warm SST bias that is as large as 10 °C along the coast of California in the boreal summer season and this warm bias is significantly corrected by the coupled downscaling. The CPL simulated climatological upwelling cold tongue is shown to be comparable to the corresponding observed AVHRR climatology at 4 km. The variation in the CCSM3 monthly SST is found to be very poor in comparison with the AVHRR SST in the summer months along the coast of California.

Validated against the buoy observation and COOP observation, the T2m from the UNCPL shows unrealistic seasonal variation. It exhibits too strong of a seasonal cycle during the strong upwelling season (May–September), while the seasonal variation of the T2m from the CPL run matches the observation very well. The bias and RMSE of the 10-m wind speed in the summer against the buoy observation in the CPL is 20 % less than that in the UNCPL run. The impact of the air-sea coupling on the temperature and specific humidity is largest near the surface (1,000 hPa), and it becomes weaker upward. However, the coupling impact on the wind speed is largest at a height of 850 hPa. The summer PBLH climatology from the UNCPL is overestimated by almost 100 % along the coast of California when compared with CaRD10. In contrast, the difference in the PBLH between the CPL and the CaRD10 is much smaller. Due to the enhanced offshore sea-breeze caused by the colder coastal SST in the upwelling season, 67.3 % more CE hours and 61.2 % CE additional events are generated in the CPL run than in the UNCPL experiment.

The 10 year (1985–1994) coupled downscaling of the CCSM3 by the regional ocean-atmosphere coupled modeling system of the RSM-ROMS shows much more realistic ocean and atmospheric states than the uncoupled downscaling along the coast of California. It is highlighted that the air-sea coupling plays an important role in the simulation of the mesoscale circulation of the Catalina Eddy over Southern California Bight. It is suggested that a

regional ocean-atmosphere coupled model is essential for the climate downscaling over California. The coupled downscaling of the future climate will be discussed in our next study.

Acknowledgments Funding was provided by NOAA (ECPC: NA17RJ1231), the NSF (OCE-0960770), the California Energy Commission PIER Program, the Korea Meteorological Administration Research and Development Program under Grant CATER 2012-3084, and by the Basic Science Research Program through the National Research Foundation of Korea (NRF) funded by the Ministry of Education, Science, and Technology (2012-0000158). The views expressed herein are those of the authors and do not necessarily reflect the views of the NOAA. Supercomputing resources were provided by COMPAS at SIO and TACC via XSEDE. Two anonymous reviewers helped to improve the manuscript.

References

Bosart L (1983) Analysis of a California Catalina eddy event. Mon Weather Rev 111:1619–1633

Carson TN (1998) Mid-latitude weather system. Am Meteor Soc

Chelton DB, Xie S (2010) Coupled ocean-atmosphere interaction at oceanic mesoscales. Oceanogr Mag 23:52–69

Giorgi F, Brodeur CS, Bates GT (1994) Regional climate change scenarios over the United States produced with a nested regional climate model: spatial and seasonal characteristics. J Clim 7:375–399

Haidvogel DB, Arango HG, Hedstrom K, Beckmann A, MalanotteRizzoli P, Shchepetkin AF (2000) Model evaluation experiments in the North Atlantic Basin: simulations in nonlinear terrain-following coordinates. Dyn Atmos Oceans 32:239–281

Held IM, Soden BJ (2006) Robust responses of the hydrological cycle to global warming. J Clim 19:5686–5699

Ho C, Park T, Jun S, Lee M, Park C, Kim J, Lee S, Hong Y, Song C, Lee J (2011) A projection of extreme climate events in the 21st century over east Asia using the community climate system model 3. Asia-Pac J Atmos Sci 47(4):329–344

Hong S, Pan H (1996) Nonlocal boundary layer vertical diffusion in a medium-range forecast model. Mon Weather Rev 124:2322–2339

Hong S, Pan H (2000) Impact of soil moisture anomalies on seasonal, summertime circulation over North America in a regional climate model. J Geophys Res 105(D24):29625–29634

Hong S, Noh Y, Dudhia J (2006) A new vertical diffusion package with an explicit treatment of entrainment processes. Mon Weather Rev 134:2318–2341

Hong S, Moon NK, Lim KS, Kim JW (2010) Future climatic change scenarios over Korea using a multi-nested downscaling system: a pilot study. Asia-Pacific J Atmos Sci 46:425–435

Juang HH, Kanamitsu M (1994) The NMC nested regional spectral model. Mon Weather Rev 122:3–26

Juang HH, Hong S, Kanamitsu M (1997) The NCEP regional spectral model: an update. Bull Am Meteor Soc 78:2125–2143

Kalnay E et al (1996) The NCEP/NCAR 40-year reanalysis project. Bull Am Meteo Soc 77:437–471

Kanamaru H, Kanamitsu M (2008) Dynamical downscaling of global analysis and simulation over the northern hemisphere. Mon Weather Rev 136:2796–2803

Kanamitsu M, Kanamaru H (2007) Fifty-seven-year California reanalysis downscaling at 10 km (CaRD10). Part I: system detail and validation with observations. J Clim 20:5553–5571

Kanamitsu M, Yoshimura K, Yhang Y, Hong S (2010) Errors of interannual variability and multi-decadal trend in dynamical regional climate downscaling and its corrections. J Geophys Res 115:D17115

Kanamitsu M, Yulaeva E, Li H, Hong S (2013) Catalina Eddy as revealed by the historical downscaling of reanalysis. Asia-Pac J Atmos Sci (in press)

Koenigk T, Doscher R, Nikulin G (2011) Arctic future scenario experiments with a coupled regional climate model. Tellas 63A:69–86

Leung LR, Qian Y, Bian X, Washington WM, Han J, Roads J (2004) Mid-century ensemble regional climate change scenarios for the western United States. Clim Change 62(1–3):75–113

Li H, Kanamitsu M, Hong S (2012) California reanalysis downscaling at 10 km using an ocean-atmosphere coupled regional model system. J Geophys Res 117:D12118

Marchesiello P, McWilliams JC, Shchepetkin A (2003) Equilibrium structure and dynamics of the California current system. J Phys Oceanogr 33:753–783

Mass CF, Albright MD (1989) Origin of the Catalina Eddy. Mon Weather Rev 117:2406–2436

Mass CF, Steenburg WJ (2000) An observational and numerical study of an orographically trapped wind reversal along the west coast of the United States. Mon Weather Rev 128:2363–2397

Min H, Jhun J (2010) The change in the east asian summer monsoon simulated by the MIROC3.2 high-resolution coupled model under global warming scenarios. Asia-Pac J Atmos Sci 46:73–88

Murphy JM (1995) Transient response of the Hadley centre coupled ocean-atmosphere model to increasing carbon dioxide. Part 1: control climate and flux adjustment. J Clim 8:36–56

Seo H, Xie S (2011) Response and impact of equatorial ocean dynamics and tropical instability waves in the tropical Atlantic under global warming: a regional coupled downscaling study. J Geophys Res 116:C03026

Shchepetkin AF, McWilliams JC (2005) The regional oceanic modeling system (ROMS): a split-explicit, free-surface, topography-following-coordinate ocean model. Ocean Modell 9:347–404

Stouffer RJ, Manabe S (1999) Response of a coupled ocean-atmosphere model to increasing atmospheric carbon dioxide: sensitivity to the rate of increase. J Clim 12:2224–2237

Ulrickson BL, Hoffmaster JS, Robinson J, Vimont D (1995) A numerical modeling study of the Catalina Eddy. Mon Weather Rev 123:1364–1373

Vecchi GA, Soden BJ (2007) Global warming and the weakening of the tropical circulation. J Clim 20:4316–4340

Wang Y, Leung LR, McGregor JL, Lee D, Wang W, Ding Y, Kimura F (2004) Regional climate modeling: progress, challenges and prospects. J Meteor Soc Jpn 82:1599–1628

Washington WM, Meehl GA (1989) Climate sensitivity due to increased CO_2: experiment with a coupled atmosphere and ocean general circulation model. Clim Dyn 4:1–38

Xie S et al (2007) A regional ocean-atmosphere model for eastern pacific climate: toward reducing tropical biases. J Clim 20:1504–1522

Yoshimura K, Kanamitsu M (2009) Specification of external forcing for regional model integrations. Mon Weather Rev 137:1409–1421

Zhao Z, Chen S, Kleeman MJ, Mahmud A, Tyree M, Cayan D (2011) The impact of climate change on air quality–related meteorological conditions in California. Part I: present time simulation analysis. J Clim 24:3344–3361

Zou L, Zhou T (2011) Sensitivity of a regional ocean-atmosphere coupled model to convection parameterization over western North Pacific. J Geophys Res 116:D18106